

**Absolute ozone
absorption cross
section**

J. L. Axson et al.

**Absolute ozone absorption cross section
in the Huggins Chappuis minimum
(350–470 nm) at 296 K**

J. L. Axson^{1,2}, R. A. Washenfelder^{2,3}, T. F. Kahan¹, C. J. Young^{2,3}, V. Vaida^{1,2}, and S. S. Brown³

¹Department of Chemistry and Biochemistry, University of Colorado, Campus Box 215, Boulder, CO 80309, USA

²Cooperative Institute for Research in Environmental Sciences, 216 UCB, University of Colorado, Boulder, CO 80309, USA

³Chemical Sciences Division, National Oceanic and Atmospheric Administration, 325 Broadway, Boulder, CO 80305, USA

Received: 3 June 2011 – Accepted: 19 July 2011 – Published: 1 August 2011

Correspondence to: S. S. Brown (steven.s.brown@noaa.gov)

Published by Copernicus Publications on behalf of the European Geosciences Union.

Title Page

Abstract

Introduction

Conclusions

References

Tables

Figures

◀

▶

◀

▶

Back

Close

Full Screen / Esc

Printer-friendly Version

Interactive Discussion



Abstract

We report the ozone absolute absorption cross section between 350–470 nm, the minimum between the Huggins and Chappuis bands, where the ozone cross section is less than 10^{-22} cm². Ozone spectra were acquired using an incoherent broadband cavity enhanced absorption spectrometer, with three channels centered at 365, 405, and 455 nm. The accuracy of the measured cross section is 2%. Previous measurements vary by more than an order of magnitude in this spectral region. The measurements reported here provide much greater spectral coverage than the most recent measurements. We report a minimum absorption cross section of 3.4×10^{-24} cm² at 381.8 nm, which is 22% lower than the previously reported value. The effect of O₃ concentration and water vapor partial pressure were investigated, however there were no observable changes in the absorption spectrum most likely due to the low optical density of the complex.

1 Introduction

Weak spectral absorptions play an important role in the radiative transfer of the Earth's atmosphere and accurate measurements of these are necessary for satellite retrievals of atmospheric trace gases (Burrows et al., 1999; Bogumil et al., 2003; Petropavlovskikh et al., 2011). It has recently been recognized that weak electronic features in the near-ultraviolet (UV), which are not well known, can be important for tropospheric radical production (Waschewsky et al., 1996; Matthews et al., 2005; Vaida, 2009). Ozone (O₃) plays a key role both chemically and radiatively throughout the atmosphere, acting as an absorber and blocker of harmful UV radiation (<300 nm) in the stratosphere and as the dominant source of OH radicals through its UV photolysis. Therefore, it is essential to have accurate O₃ absorption cross sections for satellite and ground based retrievals of vertical O₃ profiles and total O₃ columns, as well as to correctly model atmospheric O₃ concentrations (Burrows et al., 1999; Bogumil et al.,

Absolute ozone absorption cross section

J. L. Axson et al.

Title Page

Abstract

Introduction

Conclusions

References

Tables

Figures



Back

Close

Full Screen / Esc

Printer-friendly Version

Interactive Discussion



2003; Petropavlovskikh et al., 2011).

Although the strong bands of O₃ have been well characterized (see review by Orphal, 2003), the absorption minimum between the Huggins and Chappuis bands at 350–470 nm is less well known, particularly the minimum region near 390 nm. Previous O₃ cross sections in this region have been measured using high resolution Fourier transform spectrometers (Brion et al., 1998; Voigt et al., 2001) and grating spectrometers (Burkholder et al., 1994; Burrows et al., 1999; Bogumil et al., 2003). These studies report cross sections that differ by more than an order of magnitude near the minimum, and also show some disagreement where the cross section is greater (e.g. 8 % at 350 nm and 20 % at 450 nm). These studies have also shown that the spectra, with their large discrepancies, are highly temperature dependent (Brion et al., 1993; Burkholder et al., 1994; Burrows et al., 1999; Voigt et al., 2001; Bogumil et al., 2003). Table 1 summarizes the results of prior studies, and gives their spectral range, spectral resolution, temperature, and measured cross sections. The importance of O₃ absorption in the atmosphere, and the large discrepancies in the current literature over a wide spectral region around the O₃ minimum absorption, highlight the need for more accurate measurements of these very weak absorption cross sections.

Incoherent broadband cavity enhanced absorption spectroscopy (IBBCEAS) is a recently developed, highly sensitive method to measure trace gases and weak absorption cross sections (Fiedler et al., 2003). IBBCEAS instruments consist of an intense broadband light source, such as an arc lamp or light emitting diode (LED), high-finesse optical cavity, and multichannel detector. The pathlength generated by the optical cavity can be several tens of kilometers, making IBBCEAS more sensitive than traditional spectroscopic techniques. This increased optical path length is balanced by a reduction in intensity throughput, such that the sensitivity increase is only realized for sufficiently bright input light sources. This technique was first described in the literature by Fiedler et al. (2003), and has subsequently been used for spectroscopic measurements of NO₂, NO₃, CHOCHO, HONO, and other trace gasses (Venables et al., 2006; Langridge et al., 2006; Gherman et al., 2008; Langridge et al., 2008; Vaughan et al., 2008;

Absolute ozone absorption cross section

J. L. Axson et al.

Title Page

Abstract

Introduction

Conclusions

References

Tables

Figures



Back

Close

Full Screen / Esc

Printer-friendly Version

Interactive Discussion



Washenfelder et al., 2008; Thalman et al., 2010). More recently, Chen et al. (2011) used an IBBCEAS with an arc lamp to measure the O₃ cross section in the near-UV from 335–375 nm.

In this investigation, an IBBCEAS instrument with three channels centered at 365, 405, and 455 nm channels was designed, constructed, and characterized to measure O₃ absorption cross sections in the region between the Huggins and Chappuis bands, from 350 to 470 nm. The increased sensitivity of this instrument compared to single-pass or multi-pass cells allows for the measurement of these weak absorption cross sections with higher signal to noise and accuracy. Calibrations are based on 253.7 nm absorption of O₃ (Hg line) and Rayleigh scattering cross sections of pure gases, as described below. Both analytical standards are known to high accuracy. These results are compared to the previous literature studies of O₃ cross sections in this region.

2 Experimental

2.1 Description of the IBBCEAS instrument

The IBBCEAS used to measure O₃ absorption cross sections from 350 to 470 nm is shown in Fig. 1a. Each channel consists of an LED, lenses, a cavity composed of high-reflectivity mirrors, and an optical filter. An optical fiber connects the spectral output to a grating spectrometer with a CCD array detector. Three cavities were required to span the range of interest for the O₃ minimum. The spectral bandwidth for any single cavity is defined both by the emission spectrum of the LED light source, the useful bandwidth of the high reflectivity mirrors, and any optical filtering requirements, as described further below. The broadband radiation was supplied by LEDs centered at 365 nm (Nichia NCSU033A(T) UV LED), 405 nm (LedEngin, Inc., LZ1-00UA05) and 455 nm (LedEngin, Inc., LZ1-00DB05) powered by custom-built, constant current DC power supplies controlled at 0.5, 0.7, and 1.0 A respectively. Each LED was mounted on a temperature-controlled block with a servoed thermoelectric cooler (Watlow, EZ-

Absolute ozone absorption cross section

J. L. Axson et al.

Title Page

Abstract

Introduction

Conclusions

References

Tables

Figures

⏪

⏩

◀

▶

Back

Close

Full Screen / Esc

Printer-friendly Version

Interactive Discussion



ZONE[®] PM) and maintained at 293 K. Radiation was collimated and coupled into each of the 100 cm long cavities using a 2'' diameter F/1.2 lens. The cavities were formed using highly reflective mirrors (Advanced Thin Films) with 1 m radius of curvature. The center wavelengths and maximum reflectivities were 362 nm ($R = 0.99975$), 405 nm ($R = 0.99994$), and 455 nm ($R = 0.99993$). The corresponding effective path lengths (i.e. e^{-1}) were 4.0 km, 17 km, and 14 km respectively, when the cavities contained pure helium (He). Apertures of 1.5 cm diameter were used at the entrance and exit of each cavity to prevent light transmission at the uncoated edges of the 2.5 cm cavity mirrors.

Upon exiting the cavity, the light passes through a quartz beam splitter that was used to turn the beam of a HeNe laser through the cavity for alignment purposes. A 1'' F/3 lens collimates the exiting radiation onto an optical fiber. Bandpass filters were used on each of the optical fibers to prevent stray light from entering the spectrometer. The center wavelength and full width at half maximum (FWHM) for the bandpass filters were 360 nm with FWHM of 50 nm (Omega Optical 360WB50); 400 nm with FWHM of 70 nm (Andover Corp. 400FS70-25) or 40 nm (ThorLabs, FB400-40); and 450 nm with FWHM of 40 nm (Thorlabs, FB450-40). The optical fibers were coupled to a fiber bundle that was input to a Czerny-Turner grating spectrometer with CCD detector (Acton InSpectrum 150), as described in detail by Washenfelder et al. (2008). The fiber bundle illuminates two separate regions of the CCD, allowing spectra from two independent channels to be measured simultaneously. The spectrometer was configured with a 20 μm slit width and 1200 groove/mm grating (500 nm blaze), giving a spectral range of ~ 117 nm. Spectra of the three channels covering the 350–470 nm spectral region were acquired in two separate experiments. The grating was rotated to give a useful spectral range from 331 to 451 nm while measuring the 365 nm and 405 nm channels, and spectral range from 365 to 484 nm while measuring the 405 nm and 455 nm channels.

The wavelength calibration of the spectrometer was determined using an Hg/Ar calibration lamp with lines at 334.15, 404.66, 407.78, and 435.83 nm. The fixed slit width of 20 μm was found to give a nearly Gaussian lineshape. The FWHM increased linearly

Absolute ozone absorption cross section

J. L. Axson et al.

[Title Page](#)[Abstract](#)[Introduction](#)[Conclusions](#)[References](#)[Tables](#)[Figures](#)[◀](#)[▶](#)[◀](#)[▶](#)[Back](#)[Close](#)[Full Screen / Esc](#)[Printer-friendly Version](#)[Interactive Discussion](#)

with wavelength (but is constant in frequency space) for the two wavelength determinations. For the 365 nm and 405 nm cavity experiment, the FWHM was 0.27 nm at 350 nm and 0.51 nm at 430 nm. For the 405 nm and 455 nm cavity experiment, the FWHM was 0.29 nm at 380 nm and 0.50 nm at 470 nm.

The sample cells were cylindrical aluminum cells of 2.2 cm inner diameter centered on the optical cavities with ports for the introduction and exhaust of the sample gas. To verify the O₃ transmission through the cells, the O₃ concentration entering and exiting the cells was measured and it was determined there was no loss to the walls. In addition, there was no evidence of other features in the spectrum, and only those of O₃ were observed. The ports were immediately adjacent to the end mirrors, such that there was no purge volume used between the mirrors and the sample, as have often been employed in previous field and laboratory IBBCEAS and cavity ring down (CRDS) experiments (Brown et al., 2000; Dube et al., 2006). To stabilize the cavities, mounts with 2.0 cm graphite rods were used. Temperature and pressure in the cavities were measured at the connection between the two IBBCEAS cavities. A thermocouple monitored the temperature, which ranged from 295.1–295.8 K and a transducer (Honeywell, PPT0015AXN5V) monitored pressure, which ranged from 820.7–830.8 hPa.

2.2 Ozone generation, delivery, and measurement with a single-pass cell

The sampling set up for O₃ generation and delivery is shown in Fig. 1c. O₃ was generated by flowing oxygen (O₂), between 1–50 standard cm³ min⁻¹ (SSCM) with a mass flow controller (Alicat Scientific, MC-20SSCM-D-DB15/5m), through a discharge source (OzoneLabs, OL80) capable of generating up to 2% O₃. The O₃ concentration was diluted into a controlled flow of 1.5 standard l min⁻¹ (SLPM) of He via a second mass flow controller (Alicat Scientific, MC-5SLPM-D-DB15/5m) to produce O₃ concentration in the range of 58–1178 parts per million (ppm) (1.2×10¹⁵–2.4×10¹⁶ molecules cm⁻³). All experiments were conducted using a bath gas of He, which has a much smaller Rayleigh scattering cross section than nitrogen (N₂) or O₂ (Bodhaine

Absolute ozone absorption cross section

J. L. Axson et al.

Title Page

Abstract

Introduction

Conclusions

References

Tables

Figures

◀

▶

◀

▶

Back

Close

Full Screen / Esc

Printer-friendly Version

Interactive Discussion



et al., 1999) providing lower loss cavities with longer effective path lengths and higher sensitivity to optical absorption. Zero air and O₂ were avoided as bath gases due to the formation of O₄, which is easily observable in the 350–470 nm region (Greenblatt et al., 1990). The O₄ absorption associated with the small concentration of O₂ resulting from the dilution of the flow from the discharge source provided a negligible absorption interference as described further below. A combination of a second mass flow controller and scroll pump controlled a 1.0 SLPM flow of gases through the IBBCEAS. The excess flow of approximately 0.5 SLPM was vented to the atmosphere to maintain near-ambient pressure during all experiments. Instrument zeros consisted of a spectrum of He and were recorded by diverting the small flow of O₃ in O₂ from the discharge source to the exhaust using a three way valve.

O₃ concentrations were measured simultaneously at the same acquisition rate as the IBBCEAS spectral measurements using a single-pass absorption measurement at 254 nm, that consisted of a 10.6 cm glass cell with quartz windows, a mercury penray lamp (UVP 90-0012-01), and gallium phosphide (GaP) photodiode detector (Thorlabs SM05PD7A) with a 254 nm band pass filter (Fig. 1b). The intensity of the photodiode was measured using an analog to digital interface (Measurement Computing USB-1408FS) and recorded in the data acquisition software. A dark background was first taken of the GaP photodiode to determine its internal noise (*i*). Following this, the diode signal was recorded for each of the He blanks (*I*₀) and each of the O₃ spectra (*I*). The signal was then averaged and Eq. (1) was used to determine the O₃ concentration, where *l* is the length of the absorption cell and the O₃ cross section, $\sigma_{O_3} = 1.141 \times 10^{-17} \text{ cm}^2 \text{ molecule}^{-1}$ at 253.7 nm, was taken from Orphal (2003).

$$[O_3] = \frac{\ln\left(\frac{I_0 - i}{I - i}\right)}{(l \times \sigma)} \quad (1)$$

The quoted uncertainty in the literature O₃ absorption cross section is 0.9 % (Orphal, 2003). Our results for the 350–470 nm absorption cross section scale directly with the

**Absolute ozone
absorption cross
section**

J. L. Axson et al.

Title Page

Abstract

Introduction

Conclusions

References

Tables

Figures

◀

▶

◀

▶

Back

Close

Full Screen / Esc

Printer-friendly Version

Interactive Discussion



choice of cross section at 253.7 nm. The O₃ measurement was validated against a UV photometric O₃ instrument (Thermo Electron Corp., Model 49i, 102474-00) over the range of 50–165 ppm of O₃ and the two agreed to within 1.0%, with a slope of 1.01±0.01 and $r^2 = 0.9995$. Thus, we anticipate error on the order of 2% for the determination of the O₃ concentration itself.

2.3 Consideration of O₄ interference

As noted in the previous section, collision induced oxygen dimers, or O₄, absorb in the UV and visible spectral regions (Greenblatt et al., 1990), and are a potential spectroscopic interference for measurement of weak O₃ absorptions. The O₂/O₃ flow from the discharge source was diluted with He (Fig. 1b), such that only up to 3.3% of flow through the IBBCEAS cells was from the O₃ source, of which, at most 1.8% could consist of the O₄. Using Greenblatt et al. (1990) cross sections for O₄ of 4.1×10^{-46} , 2.4×10^{-46} , and 0.57×10^{-46} cm⁵ molecules⁻² at 360.5, 380.2, and 446.7 nm respectively and our experimental temperature and pressure, we calculate the expected O₄ optical density. For a maximum O₄ number density of 3.7×10^{17} molecules cm⁻³, the corresponding optical extinctions, α_{O_4} , are 5.6×10^{-11} , 3.3×10^{-11} , and 7.4×10^{-12} cm⁻¹ at 360.5, 380.2, and 446.7 nm, respectively. These optical extinctions are more than five orders of magnitude smaller than those that would be observed for O₃ at the same concentration, therefore, any O₄ interferences were considered negligible.

2.4 Operation of IBBCEAS Instrument

The IBBCEAS instrument required approximately 30 min of warm up to allow the temperature of the LEDs, O₃ generator, and spectrometer to stabilize. Dark background spectra were acquired to correct for the pixel-dependent dark signal. These were scaled to the integration time and subtracted from subsequent sample spectra. Absolute measurement of optical extinction by IBBCEAS requires calibration of the mirror reflectivity, or, alternatively total cavity loss. For our apparatus, this calibration is based

Absolute ozone absorption cross section

J. L. Axson et al.

Title Page

Abstract

Introduction

Conclusions

References

Tables

Figures

⏪

⏩

◀

▶

Back

Close

Full Screen / Esc

Printer-friendly Version

Interactive Discussion



on Rayleigh scattering cross sections of pure gases. Following the acquisition of the dark background, spectra of He (I_{He}) and N₂ (I_{N_2}) were taken to determine the mirror reflectivity associated with each of the IBBCEAS cavities using Eq. (2) (Washenfelder et al., 2008).

$$\frac{1 - R(\lambda)}{d} = \frac{\left(\frac{I_{N_2}}{I_{He}}\right) \alpha_{Ray}^{N_2} - \alpha_{Ray}^{He}}{1 - \frac{I_{N_2}}{I_{He}}} \quad (2)$$

where R is reflectivity, λ is wavelength, d is the cavity length, and α is extinction.

The Rayleigh scattering cross sections (σ_{Ray}) were taken from Bodhaine et al. (1999) and analysis of the spectra was done using Eq. (3) (Washenfelder et al., 2008). The factor $(1 - R(\lambda))/d$, was used directly from this calibration to derive concentrations rather than the mirror reflectivity itself. The Rayleigh scattering calibrations are accurate to within 3%. This accuracy is based on the $\pm 3\%$ accuracy of the Rayleigh N₂ cross sections compared to the measured values (Naus et al., 2000; Sneep et al., 2005) (the uncertainty of the Rayleigh scattering cross section for He is similar, but makes a minor contribution to the total uncertainty) and the 3% repeatability of successive reflectivity measurements. Example spectra and calculated reflectivities are shown in Fig. 2.

Following calibration of total cavity loss, spectra of O₃ in He ($I(\lambda)$) at various concentrations were acquired alternately with spectra of pure He ($I_0(\lambda)$). Optical extinction due to O₃ (the product of number density and cross section) was then determined as follows.

$$\alpha_{abs}(\lambda) = [O_3] \sigma_{O_3} = \left(\frac{1 - R(\lambda)}{d} + \alpha_{Ray}(\lambda) \right) \left(\frac{I_0(\lambda) - I(\lambda)}{I(\lambda)} \right) \quad (3)$$

Spectra were integrated for 1.5 s and the average of 180 spectra was recorded. The optimum integration time for the O₃ spectra between successive zeros in He was determined from an Allan deviation analysis which measures the stability of the measurement, due to noise, over time (Fig. 3a). It was determined that alternating 5 min He and

Absolute ozone absorption cross section

J. L. Axson et al.

Title Page

Abstract

Introduction

Conclusions

References

Tables

Figures

◀

▶

◀

▶

Back

Close

Full Screen / Esc

Printer-friendly Version

Interactive Discussion



**Absolute ozone
absorption cross
section**J. L. Axson et al.

[Title Page](#)[Abstract](#)[Introduction](#)[Conclusions](#)[References](#)[Tables](#)[Figures](#)[Back](#)[Close](#)[Full Screen / Esc](#)[Printer-friendly Version](#)[Interactive Discussion](#)

O_3 spectra, at or just beyond the minimum in the Allan deviation plot, was optimal. The stability of the optical cavity alignment itself was most likely responsible for the upward trend in the Allan deviation plot after 5 min since independent tests of the stability of the LEDs by a separate photodiode showed its output to be stable over a longer period of time (Fig. 3b). Similar to the reflectivity spectra, O_3 spectra were integrated for 1.5 s and 180 spectra were averaged.

The O_3 spectrum from this work was obtained by averaging roughly one hour of O_3 spectra recorded simultaneously for the 365 nm and 405 nm cavities or the 405 nm and 455 nm cavities.

3 Results and discussion

3.1 Absolute absorption cross section of O_3

Fig. 4 shows the O_3 absorption cross section measured at 295 K and 820 hPa, together with previously measured cross sections (Burkholder et al., 1994; Brion et al., 1998; Burrows et al., 1999; Voigt et al., 2001; Bogumil et al., 2003; Fuchs et al., 2009; Chen et al., 2011). Plots of the optical extinction for single CCD pixels measured at various concentrations (Fig. 5) were used to compare the derived absorption cross sections to the experimental absorption cross sections seen in Fig. 4, and to test the linearity of the IBBCEAS response over a range larger than one order of magnitude in O_3 . The cross sections determined from Fig. 4 are $\sigma_{O_3} = 3.96 \times 10^{-23} \text{ cm}^2$ at 365.1 nm, $\sigma_{O_3} = 1.51 \times 10^{-23} \text{ cm}^2$ at 405.2 nm, and $\sigma_{O_3} = 1.92 \times 10^{-22} \text{ cm}^2$ at 455.1 nm. From the linear fits and standard deviations shown in Fig. 5, we determined a maximum precision of 3% for our O_3 cross sections, although this varies with wavelength because the signal to noise varies with wavelength due to changes in LED intensity and cavity transmission.

The 365 nm and 405 nm spectra converge at 384 nm, a region where, as Fig. 2 shows, each channel has somewhat worse signal to noise and where there is only a

small region of overlap. Thus, we have the least confidence over this range because of the lower signal to noise in the spectra. The overlap between the two channels spans a small, 1.7 nm region, from 383.4 nm to 385.1 nm.

There were two sets of 405 nm spectra taken for the simultaneous measurement of the 365 nm and 405 nm cavities and the 405 nm and 455 nm cavities. Different band pass filters were used for the 405 nm cavity in each measurement to prevent out-of-band light from saturating the CCD detector. When paired with the 365 nm cavity, the 405 nm spectrum extended from 380 nm to 441.3 nm, and when paired with the 455 nm cavity, the 405 nm spectrum extended from 380 nm to 427.9 nm. To average the two sets of 405 nm spectra over the region from 380 nm to 427.9 nm, the two wavelengths were interpolated. This left out a portion of the 405 nm spectra from 427.9 nm to 441.3 nm. To obtain the full spectral coverage from 380–441.3 nm, the difference in the spectrum from 380 nm to 427.9 nm and the spectrum from 427.9 nm to 441.3 nm, was added to the latter to account for the averaging. The 455 nm cavity spectrum converged with the 405 nm cavity spectrum at 441.3 nm.

In this very weakly absorbing region between the Huggins and Chappuis bands, there is more than an order of magnitude difference in the various reported O_3 cross sections (Brion et al., 1998; Burrows et al., 1999; Voigt et al., 2001; Bogumil et al., 2003). Our reported spectrum agrees quantitatively with prior literature values at the edges of the spectrum. Our measurements are consistent most with Brion et al. (1998) and Chen et al. (2011) (not shown) with the exception of the minimum region from 375–390 nm. Our absorption cross section shows a lower minimum in this range. In addition, more defined O_3 structural features were observed in this work, Brion et al. (1998), and Chen et al. (2011) when compared to the other literature cross sections (Burrows et al., 1999; Voigt et al., 2001; Bogumil et al., 2003). The measurements also agree within 0.5% at 404 nm with Fuchs et al. (2009), in which CRDS was used to measure the O_3 cross section, with the highest precision currently available within this wavelength range, to quantify its interference associated with measurements of NO_2 at the single wavelength of a diode laser.

**Absolute ozone
absorption cross
section**

J. L. Axson et al.

Title Page

Abstract

Introduction

Conclusions

References

Tables

Figures

◀

▶

◀

▶

Back

Close

Full Screen / Esc

Printer-friendly Version

Interactive Discussion



**Absolute ozone
absorption cross
section**

J. L. Axson et al.

Title Page

Abstract

Introduction

Conclusions

References

Tables

Figures

◀

▶

◀

▶

Back

Close

Full Screen / Esc

Printer-friendly Version

Interactive Discussion



Though the O_3 cross sections derived in this work agree best with the data of Brion et al. (1998), there is some disagreement between their spectra and ours near the minimum absorption at 375–390 nm. This is the region where the largest discrepancies have been reported. Prior to the measurements in this work, the lowest reported O_3 cross section were those of Brion et al. (1998) at 377.5 nm with a $\sigma_{O_3} = 4.4 \times 10^{-24} \text{ cm}^2$. Chen et al. (2011) examined the near-UV region from 335–375 nm, just to the short wavelength side of the minimum. These authors suggested that the absorption cross section in this region would be even lower than seen in previous studies (Brion et al., 1998; Burrows et al., 1999; Voigt et al., 2001; Bogumil et al., 2003; Chen et al., 2011). In this work, the minimum was observed to be lower than the Brion et al. (1998) value, at 381.8 nm with $\sigma_{O_3} = 3.4 \times 10^{-24} \text{ cm}^2$.

3.2 Pressure and relative humidity effect on O_3

It has been suggested that O_3 cross sections could be sensitive to the molecular environment (Vaida et al., 1989; Frost et al., 1995; Vaida et al., 2000). At the low partial pressures of O_3 used, ranging from 1.2×10^{15} – 2.4×10^{16} molecules cm^{-3} , there was no evidence of non linear O_3 partial pressure dependence. Although the total pressure was the ambient atmospheric pressure, Orphal (2003) notes in his review that there was no experimental or theoretical evidence of pressure dependence in the O_3 cross section in the region of interest.

Modeling studies by Frost et al. (1995) predict that O_3 will form $O_3 \cdot H_2O$ clusters that will absorb more strongly than O_3 in the region between 350 and 470 nm. The photolysis of $O_3 \cdot H_2O$ was evaluated based on spectroscopic and photofragment experiments which measured OH formation on photolysis of $O_3 \cdot H_2O$ (Hurwitz et al., 1995). Photolysis of this complex is suggested by Vaida (2009) and Frost et al. (1995) to be important in the atmosphere because the $O_3 \cdot H_2O$ cluster can act as an additional atmospheric source of OH radicals. The cross section of the $O_3 \cdot H_2O$ cluster is predicted to be 1–4 orders of magnitude more than that for O_3 , but has never been measured experimentally. With the IBBCEAS instrument, we attempted to observe the change in cross

section of O₃ using relative humidities (RH) of up to 90%. The product of the cluster number density and its cross section at the wavelengths of interest here is below the signal to noise of the experiment and yielded no absorption due to the O₃·H₂O complex. We calculate based on Frost et al. (1995) that the ratio of the O₃·H₂O complex concentration to the O₃ concentration is 4.3×10^{-6} , and this is below the detection limit of our experiment.

4 Conclusions

Using a newly developed, high sensitivity IBBCEAS instrument, we measured the O₃ absolute absorption cross section from 350–470 nm at 295 K and 820 hPa with low O₃ partial pressures. These measurements directly address the large discrepancy in current literature cross sections in this region and agree well with the most recent measurements that are based on cavity enhanced methods which measured a portion of this spectral region. We also find the minimum absorption cross section from 380–386 nm to be 22 % lower than the lowest previously reported value. The effect of ozone concentration and relative humidity were investigated without any effect observed on the absorption cross section of O₃. The absorption cross sections obtained here may be useful for applications such as satellite retrievals, ground-based O₃ monitoring, and atmospheric radiative transfer models. Future work may include temperature dependent measurements, since the O₃ cross section across this minimum is known to be strongly temperature dependent.

Acknowledgements. We thank Rich McLaughlin for machining custom mirror mounts for the IBBCEAS instrument. We thank Steve Ciciora for designing custom DC power supplies and amplifiers. All authors acknowledge funding from CIRES Innovative Research Program. JLA acknowledges support from the NASA Earth and Space Science Fellowship. VV acknowledges funding from NSF CHE 1011770. CJY and TFK thank NSERC for PDF scholarships.

Absolute ozone absorption cross section

J. L. Axson et al.

Title Page

Abstract

Introduction

Conclusions

References

Tables

Figures

◀

▶

◀

▶

Back

Close

Full Screen / Esc

Printer-friendly Version

Interactive Discussion



References

- Bodhaine, B. A., Wood, N. B., Dutton, E. G., and Slusser, J. R.: On Rayleigh optical depth calculations, *J. Atmos. Ocean. Technol.*, 16, 1854–1861, 1999.
- 5 Bogumil, K., Orphal, J., Homann, T., Voigt, S., Spietz, P., Fleischmann, O.C., Vogel, A., Hartmann, M., Kromminga, H., Bovensmann, H., Frerick, J., and Burrows, J. P.: Measurements of molecular absorption spectra with the SCIAMACHY pre-flight model: instrument characterization and reference data for atmospheric remote-sensing in the 230–2380 nm region, *J. Photochem. Photobiol. A-Chem.*, 157, 167–184, 2003.
- 10 Brion, J., Chakir, A., Daumont, D., Malicet, J., and Parisse, C.: High-resolution laboratory absorption cross-section of O₃ – Temperature effect, *Chem. Phys. Lett.*, 213, 610–612, 1993.
- Brion, J., Chakir, A., Charbonnier, J., Daumont, D., Parisse, C., and Malicet, J.: Absorption spectra measurements for the ozone molecule in the 350–830 nm region, *J. Atmos. Chem.*, 30, 291–299, 1998.
- 15 Brown, S. S., Wilson, R. W. and Ravishankara, A. R.: Absolute intensities for third and fourth overtone absorptions in HNO₃ and H₂O₂ measured by cavity ring down spectroscopy, *J. Phys. Chem. A*, 104, 4976–4983, 2000.
- Burkholder, J. B. and Talukdar, R. K.: Temperature-dependence of the ozone absorption-spectrum over the wavelength range 410 to 760 nm, *Geophys. Res. Lett.*, 21, 581–584, 1994.
- 20 Burrows, J. P., Richter, A., Dehn, A., Deters, B., Himmelmann, S., and Orphal, J.: Atmospheric remote-sensing reference data from GOME – Part 2. Temperature-dependent absorption cross sections of O₃ in the 231–794 nm range, *J. Quant. Spectrosc. Radiat. Transf.*, 61, 509–517, 1999.
- Chen, J. and Venables, D. S.: A broadband optical cavity spectrometer for measuring weak near-ultraviolet absorption spectra of gases, *Atmos. Meas. Tech.*, 4, 425–436, doi:10.5194/acp-4-425-2011, 2011.
- 25 Dube, W. P., Brown, S. S., Osthoff, H. D., Nunley, M. R., Ciciora, S. J., Paris, M. W., McLaughlin, R. J., and Ravishankara, A. R.: Aircraft instrument for simultaneous, in situ measurement of NO₃ and N₂O₅ via pulsed cavity ring-down spectroscopy, *Rev. Sci. Instrum.*, 77, 1–11, 2006.
- 30 Fiedler, S. E., Hese, A., and Ruth, A. A.: Incoherent broad-band cavity-enhanced absorption spectroscopy, *Chem. Phys. Lett.*, 371, 284–294, 2003.
- Frost, G. J. and Vaida, V.: Atmospheric implications of the photolysis of the ozone-water weakly

Absolute ozone absorption cross section

J. L. Axson et al.

Title Page

Abstract

Introduction

Conclusions

References

Tables

Figures

◀

▶

◀

▶

Back

Close

Full Screen / Esc

Printer-friendly Version

Interactive Discussion



**Absolute ozone
absorption cross
section**

J. L. Axson et al.

[Title Page](#)[Abstract](#)[Introduction](#)[Conclusions](#)[References](#)[Tables](#)[Figures](#)[◀](#)[▶](#)[◀](#)[▶](#)[Back](#)[Close](#)[Full Screen / Esc](#)[Printer-friendly Version](#)[Interactive Discussion](#)

bound complex, *J. Geophys. Res.-Atmos.*, 100, 18803–18809, 1995.

Fuchs, H., Dube, W. P., Lerner, B. M., Wagner, N. L., Williams, E. J., and Brown, S. S.: A sensitive and versatile detector for atmospheric NO₂ and NO_x based on blue diode laser cavity ring-down spectroscopy, *Environ. Sci. Technol.*, 43, 7831–7836, 2009.

5 Gherman, T., Venables, D. S., Vaughan, S., Orphal, J., and Ruth, A. A.: Incoherent broadband cavity-enhanced absorption spectroscopy in the near-ultraviolet: Application to HONO and NO₂, *Environ. Sci. Technol.*, 42, 890–895, 2008.

Greenblatt, G. D., Orlando, J. J., Burkholder, J. B., and Ravishankara, A. R.: Absorption-measurements of oxygen between 330 nm and 1140 nm, *J. Geophys. Res.-Atmos.*, 95, 18577–18582, 1990.

10 Hurwitz, Y. and Naaman, R.: Production of OH by dissociating ozone water complexes at 266 nm and 355 nm by reacting O(D⁻¹) with water dimers, *J. Chem. Phys.*, 102, 1941–1943, 1995.

Langridge, J. M., Ball, S. M., and Jones, R. L.: A compact broadband cavity enhanced absorption spectrometer for detection of atmospheric NO₂ using light emitting diodes, *Analyst*, 131, 916–922, 2006.

15 Langridge, J. M., Ball, S. M., Shillings, A. J. L., and Jones, R. L.: A broadband absorption spectrometer using light emitting diodes for ultrasensitive, in situ trace gas detection, *Rev. Sci. Instrum.*, 79, 123110, 2008.

20 Matthews, J., Sinha, A., and Francisco, J. S.: The importance of weak absorption features in promoting tropospheric radical production, *Proc. Natl. Acad. Sci. USA*, 102, 7449–7452, 2005.

Naus, H. and Ubachs, W.: Experimental verification of Rayleigh scattering cross sections, *Opt. Lett.*, 25, 347–349, 2000.

25 Orphal, J.: A critical review of the absorption cross-sections of O₃ and NO₂ in the ultraviolet and visible, *J. Photochem. Photobiol. A-Chem.*, 157, 185–209, 2003.

Petrovavlovskikh, I., Evans, R., Mcconville, G., Oltmans, S., Quincy, D., Lantz, K., Disterhoft, P., Stanek, M., and Flynn, L.: Sensitivity of Dobson and Brewer Umkehr ozone profile retrievals to ozone cross-sections and stray light effects, *Atmos. Meas. Tech. Discuss.*, 4, 2007–2035, doi:10.5194/amtd-4-2007-2011, 2011.

30 Sneep, M. and Ubachs, W.: Direct measurement of the Rayleigh scattering cross section in various gases, *J. Quant. Spectrosc. Radiat. Transf.*, 92, 293–310, 2005.

Thalman, R. and Volkamer, R.: Inherent calibration of a blue LED-CE-DOAS instrument to

measure iodine oxide, glyoxal, methyl glyoxal, nitrogen dioxide, water vapour and aerosol extinction in open cavity mode, *Atmos. Meas. Tech.*, 3, 1797–1814, doi:10.5194/amt-3-1797-2010, 2010.

Vaida, V.: Spectroscopy of photoreactive systems: Implications for atmospheric chemistry, *J. Phys. Chem. A*, 113, 5–18, 2009.

Vaida, V. and Headrick, J. E.: Physicochemical properties of hydrated complexes in the Earth's atmosphere, *J. Phys. Chem. A*, 104, 5401–5412, 2000.

Vaida, V., Donaldson, D. J., Strickler, S. J., Stephens, S. L., and Birks, J. W.: A reinvestigation of the electronic-spectra of ozone condensed-phase effects, *J. Phys. Chem.*, 93, 506–508, 1989.

Vaughan, S., Gherman, T., Ruth, A. A., and Orphal, J.: Incoherent broad-band cavity-enhanced absorption spectroscopy of the marine boundary layer species I₂, IO and OIO, *Phys. Chem. Chem. Phys.*, 10, 4471–4477, 2008.

Venables, D. S., Gherman, T., Orphal, J., Wenger, J. C., and Ruth, A. A.: High sensitivity in situ monitoring of NO₃ in an atmospheric simulation chamber using incoherent broadband cavity-enhanced absorption spectroscopy, *Environ. Sci. Technol.*, 40, 6758–6763, 2006.

Voigt, S., Orphal, J., Bogumil, K. and Burrows, J. P.: The temperature dependence (203–293 K) of the absorption cross sections of O₃ in the 230–850 nm region measured by Fourier-transform spectroscopy, *J. Photochem. Photobiol. A-Chem.*, 143, 1–9, 2001.

Waschewsky, G. C. G., Horansky, R., and Vaida, V.: Effect of dimers on the temperature-dependent absorption cross section of methyl iodide, *J. Phys. Chem.*, 100, 11559–11565, 1996.

Washenfelder, R. A., Langford, A. O., Fuchs, H., and Brown, S. S.: Measurement of glyoxal using an incoherent broadband cavity enhanced absorption spectrometer, *Atmos. Chem. Phys.*, 8, 7779–7793, doi:10.5194/acp-8-7779-2008, 2008.

Absolute ozone absorption cross section

J. L. Axson et al.

Title Page

Abstract

Introduction

Conclusions

References

Tables

Figures

◀

▶

◀

▶

Back

Close

Full Screen / Esc

Printer-friendly Version

Interactive Discussion



Absolute ozone absorption cross section

J. L. Axson et al.

Table 1. Measurements of O₃ absorption cross section between 350–470 nm.

Reference	Instrumental Technique	Spectral Region (nm)	Spectral Resolution (nm)	Temperature (K)	Cross section at 365 nm ($\times 10^{-23}$ cm ²)	Cross section at 405 nm ($\times 10^{-22}$ cm ²)	Cross section at 455 nm
Burkholder and Talukdar (1994)	Grating spectrometer	410–760	0.20	298	–	–	1.99
Brion et al. (1998)	FTS	350–830	0.01	295	4.10	1.49	2.26
Burrows et al. (1999)	Grating spectrometer	230–794	0.2–0.4	293	5.96	4.26	2.42
Voigt et al. (2001)	FTS	230–851	0.027	293	7.58	7.14	2.38
Bogumil et al. (2003)	Grating spectrometer	230–1075	0.26	293	4.89	2.12	2.32
Fuchs et al. (2009)	CRDS	404	0.5	293	–	1.49	–
Chen and Venables (2011)	IBBCEAS	335–375	0.26	296	4.85	–	–
This work	IBBCEAS	350–470	0.27–0.51	295	3.96	1.51	1.92

[Title Page](#)
[Abstract](#)
[Introduction](#)
[Conclusions](#)
[References](#)
[Tables](#)
[Figures](#)
[Back](#)
[Close](#)
[Full Screen / Esc](#)
[Printer-friendly Version](#)
[Interactive Discussion](#)


Absolute ozone absorption cross section

J. L. Axson et al.

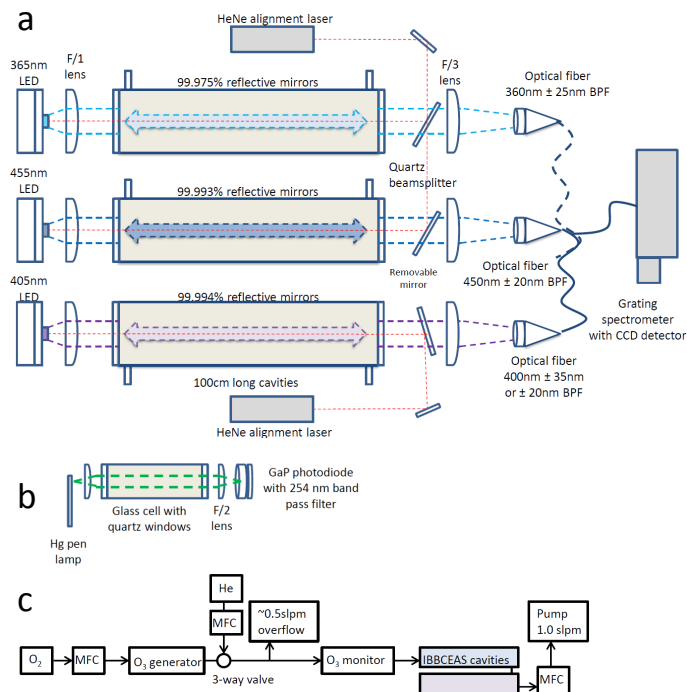


Fig. 1. (a) Schematic of the three channel IBBCEAS consisting of LED light sources, optical cavities, and a CCD detector. Also included is the O₃ generator consisting of Hg light source and GaP photodiode. (b) Schematic of the ozone monitor, consisting of Hg light source and GaP photodiode. (c) Block diagram showing O₃ delivery system to the IBBCEAS.

Title Page

Abstract

Introduction

Conclusions

References

Tables

Figures

◀

▶

◀

▶

Back

Close

Full Screen / Esc

Printer-friendly Version

Interactive Discussion



Absolute ozone absorption cross section

J. L. Axson et al.

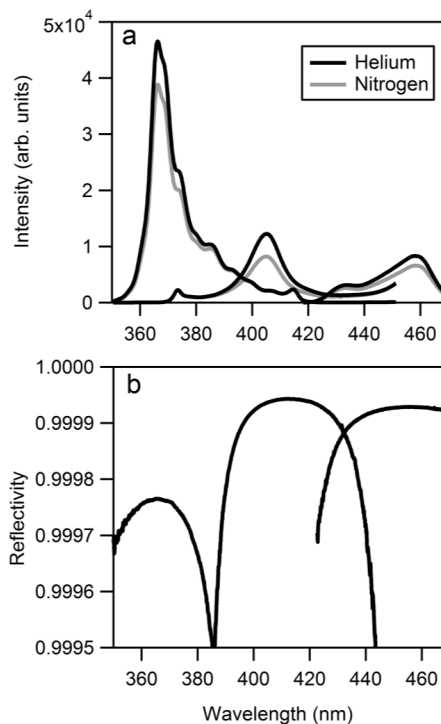


Fig. 2. (a) Example spectra of the transmitted intensity of He and N₂ through the 365 nm, 405 nm, and 455 nm IBBCEAS cavities. The structure observed for the 365 nm channel is due to the etalon structures from the 365 nm LED. (b) The derived reflectivity curves of the 365 nm, 405 nm, and 455 nm centered mirrors based on Eq. (2).

[Title Page](#)[Abstract](#)[Introduction](#)[Conclusions](#)[References](#)[Tables](#)[Figures](#)[◀](#)[▶](#)[◀](#)[▶](#)[Back](#)[Close](#)[Full Screen / Esc](#)[Printer-friendly Version](#)[Interactive Discussion](#)

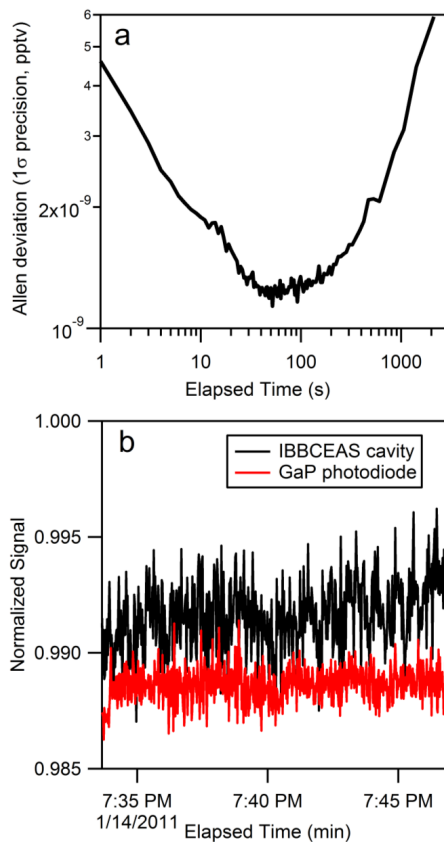


Fig. 3. (a) Allen deviation plot of the optical density of the IBBCEAS for a single pixel at 370 nm in the 365 nm channel. The minimum near 5 min, was selected as the optimum sampling time between zeros. (b) Stability of the 365 nm LED intensity using a GaP photodiode, shown together with the stability of the IBBCEAS cavities for a single pixel at 376 nm.

Absolute ozone absorption cross section

J. L. Axson et al.

Title Page

Abstract Introduction

Conclusions References

Tables Figures

◀ ▶

◀ ▶

Back Close

Full Screen / Esc

Printer-friendly Version

Interactive Discussion



Absolute ozone absorption cross section

J. L. Axson et al.

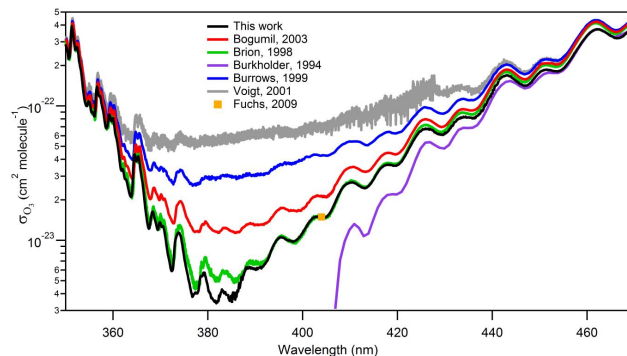


Fig. 4. The O_3 cross section from 350–470 nm determined in this work compared to other published measurements.

[Title Page](#)[Abstract](#)[Introduction](#)[Conclusions](#)[References](#)[Tables](#)[Figures](#)[⏪](#)[⏩](#)[◀](#)[▶](#)[Back](#)[Close](#)[Full Screen / Esc](#)[Printer-friendly Version](#)[Interactive Discussion](#)

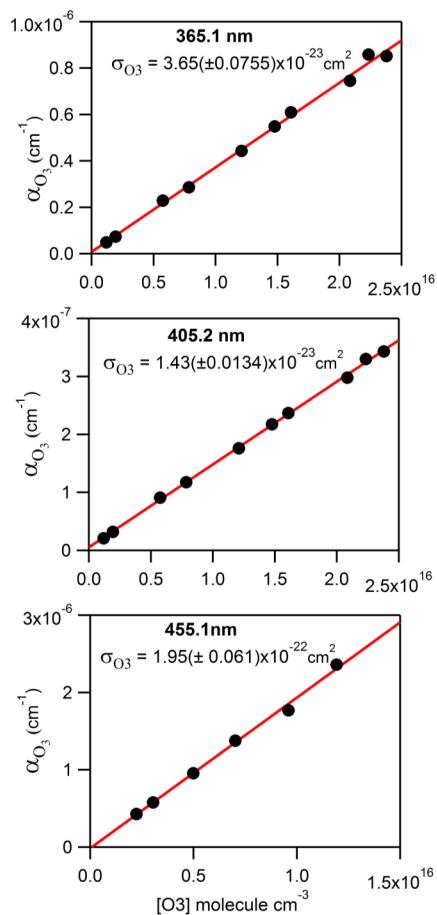


Fig. 5. Optical extinction measurements at various O₃ concentrations whose slope is the absolute absorption cross sections.

Absolute ozone absorption cross section

J. L. Axson et al.

Title Page

Abstract Introduction

Conclusions References

Tables Figures

◀ ▶

◀ ▶

Back Close

Full Screen / Esc

Printer-friendly Version

Interactive Discussion

